Original Research Paper

IJES *Iranian Journal of Earth Sciences*
Vol. 15, No. 2, 2023, 121-139.
DOI: 10.30495/ijes.2022.1941506.1657

Study of A-type granite from the South of Lake Urmia, Sanandaj-Sirjan Zone: implications for the Neotethys opening in Iran

Nasser Ashrafi[*1], Mehrdad Pourmohsen [1], Morovvat Faridazad [2]

1. Department of Geology, Payame Noor University, Tehran, Iran.
2. Mining Engineering Faculty, Sahand University of Technology, Tabriz, Iran.

Received 12 August 2022; accepted 15 November 2022

Abstract

The magmatic evidence of the Neotethys opening in Iran, such as the Late Paleozoic A-type granitoids, was mainly discovered along the Sanandaj-Sirjan Zone and parallel to the Neotethys suture. Therefore, they may provide important clues about the geodynamic evolution of the Sanandaj-Sirjan Zone. The South of Lake Urmia (SLU) granite is situated near the Khalifan A-type pluton (315±2 Ma) with a cover of the Permian sediments. The rock-forming minerals of the SLU granite consist of quartz, alkali-feldspars (K-rich and microperthitic), sodic plagioclases, biotite (Fe-rich), zircon, apatite, and Fe-Ti oxides. The chemical composition of the SLU granite is characterized by high FeO^t/MgO and (Na_2O+K_2O)/CaO ratios, which are typical features of A-type granites. Furthermore, the studied rocks exhibit the chemical characters of the A_1 subgroup of A-type granites with peraluminous and K_2O-rich affinities. On the multi-element spider plot, the SLU granite shows distinct negative Ba, Sr, P, and Ti anomalies and positive Pb anomalies. Moreover, the Chondrite-normalized rare earth elements (REE) patterns display slope downwards from LREE to HREE, with flattening at the HREE end and distinct negative Eu anomalies. The ratios of trace elements provide evidence for the contribution of the OIB-like mafic melts with crustal interactions to generate the granitic magmas of the SLU pluton. The compositional and stratigraphic features of the SLU granite are also consistent with an extensional setting during the Late Paleozoic in Iran. Therefore, the genesis of the SLU granite can be attributed to the syn-rift magmatism of the Cimmerian terranes. A comprehensive review of the Late Paleozoic rocks occurrence shows that they mainly are emerged in the northeast margin of the Sanandaj-Sirjan Zone and around the structural depressions such as Lake Urmia (so-called Tertiary fore-arc or Mesozoic back-arc).

Keywords: A-type granite, Sanandaj-Sirjan Zone, NW Iran, Neotethys opening, Late Paleozoic

1. Introduction

A-type granites are closely linked with tectonics and geodynamics; they occur in geodynamic contexts ranging from within-plate settings associated with anorogenic rifting to plate boundaries related to post-collisional extension (e.g., Eby 1992; Bonin 2004, 2007; Collins et al. 2018). However, the formation of A-type granite in mobile zones is not restricted to extensional regimes and it may be related to final consolidation in a compressional regime such as the Late Paleozoic A-type granites from Central Asia (Coleman et al. 1992). There is no agreement on the source of A-type granites up to now. They have been mainly attributed to mantle-derived magmas (Bonin and Giret 1990; Turner et al. 1992), crustal-derived magmas (Collins et al. 1982; Landenberger and Collins, 1996), or mixed sources (Eby 1990; Yang et al. 2006). A-type granites are characterized by iron-rich mafic silicates, perthitic feldspars, and alkali-rich mafic silicates in peralkaline suites. They are metaluminous to peralkaline, sometimes peraluminous with alkali-calcic to alkaline affinities, and generally produced under reducing conditions. They are also marked by high alkali, LILE, and HFSE contents, high Fe/Mg ratios, low CaO, and OIB-like compositions (e.g., Whalen et al. 1987; Eby 1990; Bonin 2007; Frost and Frost 2011; Collins et al. 2018).

---

*Corresponding author.
E-mail address (es): n_ashrafi@pnu.ac.ir

The paleogeographic reconstruction of Iran during the Late Paleozoic has always been debatable. Late Paleozoic A-type granites occur in the Turkish-Iranian plateau and provide some key evidence on the geodynamic evolution of the Tethyan oceans during Hercynian orogeny (e.g., Topuz et al. 2010; Rolland et al. 2011; Dokuz et al. 2011; Bea et al. 2011; Advay and Ghalamghash 2011; Alirezaei and Hassanzadeh 2012; Saccani et al. 2013; Shafaii Moghadam et al. 2015; Azizi et al. 2017; Honarmand et al. 2017; Mohammadi et al. 2019; Jamei et al. 2021).The Late Paleozoic A-type units of Iran are overlain by Permian to Early Mesozoic marine sediments, which is consistent with an extensional regime in the Late Palaeozoic (e.g., Shafaii Moghadam et al. 2015; Jamei et al. 2021). The extensional regime or rifting of Iran from the northern margin of Gondwana occurred during the Late Carboniferous to the late Early Permian and caused the opening of Neotethys, which was followed by the northward movement of Cimmerian terranes such as Iran, Helmand, and Tibet blocks (Stampfli and Borel 2002). The Neotethys opening in Iran has been attributed to the Late Devonian (Azizi et al. 2017; Mohammadi et al. 2019), Early Carboniferous (Saccani et al. 2013; Mohammadi et al. 2019; Jamei et al. 2021), Late Carboniferous (Bea et al. 2011; Ghaffari et al. 2013; Advay and Ghalamghash 2011; Shafaii Moghadam et al. 2015) and Early Permian (Alirezaei and Hassanzadeh 2012; Honarmand et al. 2017), based on the reported

magmatic activities especially along the Sanandaj-Sirjan Magmatic-Metamorphic Zone (SSMMZ) and parallel to the Neotethys suture (Fig 1).

This paper presents the first detailed petrographic and whole-rock geochemistry studies on the Late Paleozoic granite from the South of Lake Urmia, the northern edge of SSMMZ. In this study, we also compare the present data with the previous studies carried out on some Late Paleozoic magmatic rocks of Iran and discuss geodynamic evolution in the region with a focus on the Neotethys opening evidence.

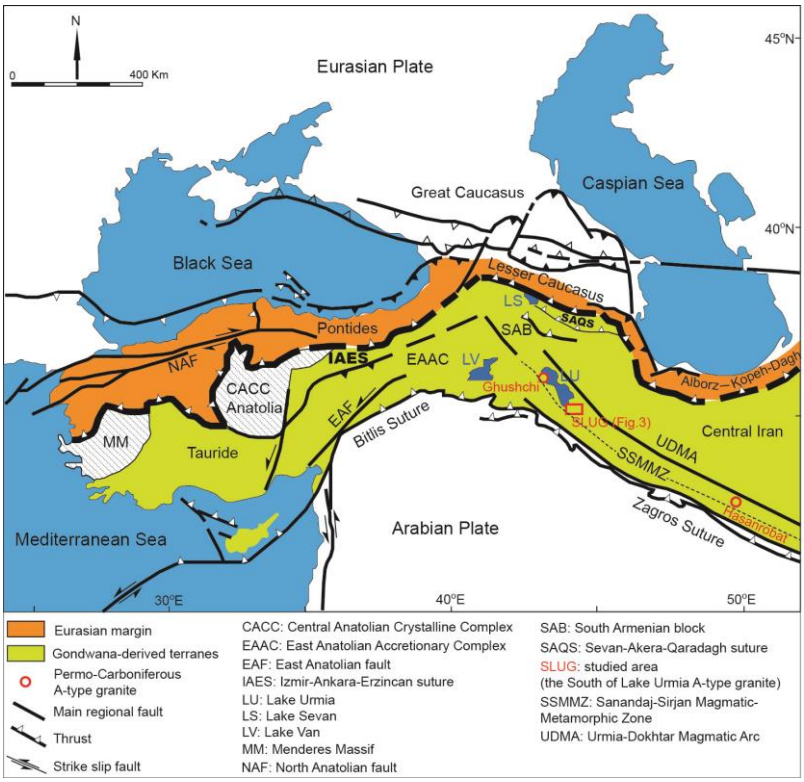

Fig 1 Structural sketch map of the Tauride-Anatolides, Caucasus and Iranian belts (modified after Sosson et al. 2010); the location of two Late Paleozoic A-type granite, also the outlines of the geological map in Figure 3, including the studied area, are shown.

2. Geological background

Iran can be divided into three major structural units based on the ophiolite-bearing sutures: the Zagros orogenic belt (southern unit), the Central Iran unit, and Kopeh-Dagh and Alborz belts (northern unit) (Berberian and King 1981). The Zagros orogenic belt consists of several NW-SE trending parallel subdivisions such as the Urmia-Dokhtar magmatic arc (UDMA), the Sanandaj-Sirjan zone (SSMMZ) and the Zagros fold-thrust belt (Fig 2).

The SSMMZ, a zone of ~1500 km long and 150-250 km wide, lies on the south of the UDMA and places between the towns of Sanandaj/Urmia in the northwest and Sirjan/Esfandaghen in the southeast (Stöcklin 1968; Takin 1972; Alavi 1994; Mohajjel and Fergusson 2000; Mohajjel et al. 2003). The SSMMZ is composed mainly of metamorphosed and intricately deformed rocks, associated with deformed/undeformed plutons and Mesozoic volcanic rocks (Mohajjel et al. 2003; Azizi and Moinevaziri 2009; Ahadnejad 2013; Chiu et al. 2013). Late Neoproterozoic to Early Cambrian (ca. 600-500 Ma) zircon U-Pb ages have been reported for the basement of the SSMMZ (e.g., Hassanzadeh et al. 2008; Azizi et al. 2011). The study area, as a part of the SSMMZ, consists of Cadomian basement, Paleozoic platform sediments, and Paleozoic to Triassic igneous rocks, which is similar to the geologic succession of Central Iran (Berberian and King 1981; Alavi 1991). The Late Neoproterozoic Kahar Formation with meta-sediments and meta-igneous rocks is common in the SSMMZ, the Central Iran unit, and the Alborz belt. It is overlain by Cambrian-Ordovician sedimentary rocks including Bayandor sandstones and shales, Soltanieh dolomites, Barut sandstones, Zaigun-Lalun sandstones and quartzites, and Mila limestones (Eftekharnejad 1973, 1980; Berberian and King 1981). The peak of magmatism in the SSMMZ was during the Mesozoic as described by Berberian and Berberian (1981) and Mohajjel et al. (2003). Several granitoid plutons have been reported from the Mesozoic magmatic arc (e.g., Ahmadi-Khalaji et al. 2007; Arvin et al. 2007; Fazlnia et al. 2007, 2009; Ghalamgash et al. 2009; Mazhari et al. 2009a, b; Shahbazi et al. 2010; Ahadnejad et al. 2011; Aliani et al. 2012; Esna-Ashari et al. 2012), which located mainly in the southwest margin of the

SSMMZ (around the outer sub-zone depicted by Mohajjel et al. (2003)). In contrast, the Paleozoic magmatism in the SSMMZ was rare and emerged mainly in the northeast margin (around the inner sub-zone depicted by Mohajjel et al. (2003)). Mafic and felsic magmatism of the Paleozoic is limited to Devonian pillow basalt associated with Sargaz metamorphic complex (Ghasemi et al. 2002), basaltic lavas in the Permian strata of Golpaygan (Thiele et al. 1968; Alirezaei and Hassanzadeh 2012), rhyolitic rocks in the Devonian-Carboniferous units of Jolfa and Ajabshir (Moayyed 2013; Delavari et al. 2019; Jamei et al. 2021), Misho gabbro (Saccani et al. 2013), Hasansalaran granite (Azizi et al. 2017), Moro granite (Mohammadi et al. 2019), Heris granite (Advay and Ghalamghash 2011), Ghazan gabbro (Asadpour et al. 2013), Hasanrobat granite (Alirezaei and Hassanzadeh 2012; Honarmand et al. 2017), Ghushchi gabbronorite and granite (Advay et al. 2010; Shafaii Moghadam et al. 2015), and Khalifan leucogranite with Late Carboniferous age (Bea et al. 2011) (Fig 2).

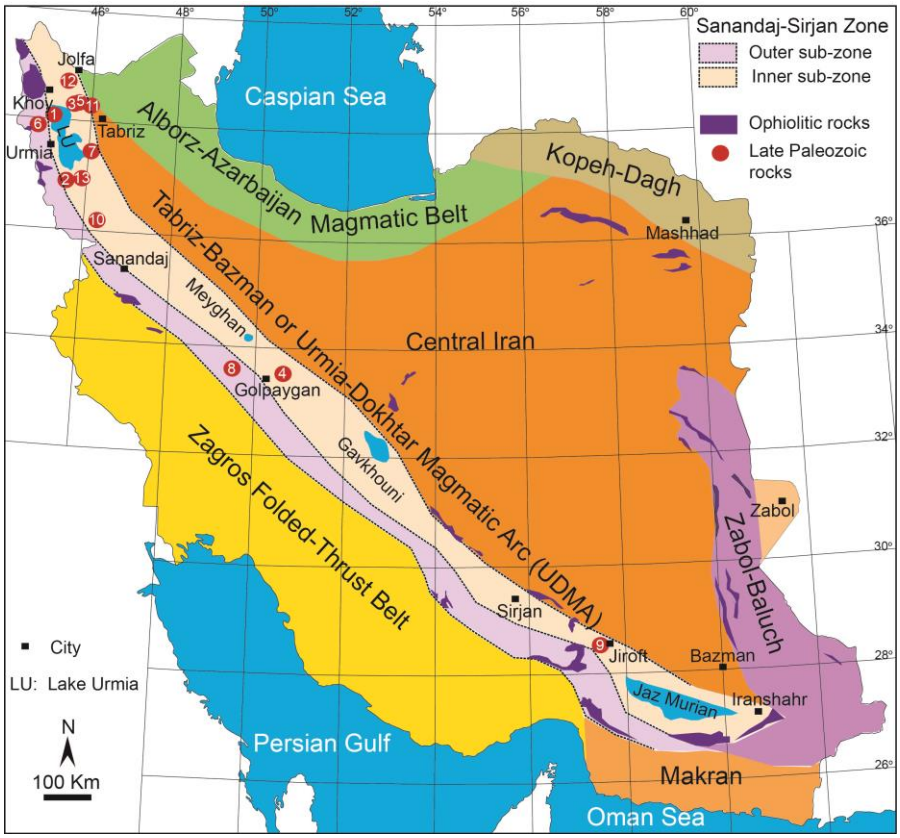

Fig 2 Major geological subdivisions of Iran (modified after Berberian and Berberian (1981); Alavi (1994); Mohajjel et al. (2003)) with the location of the reported Late Paleozoic rocks in the SSMMZ including: (1) Ghushchi (Shafaii Moghadam et al. 2015), (2) Khalifan (Bea et al. 2011), (3) Heris (Advay and Ghalamghash 2011), (4) Hasanrobat (Alirezaei and Hassanzadeh 2012), (5) Misho (Saccani et al. 2013), (6) Ghazan (Asadpour et al. 2013), (7) Ajabshir (Moayyed 2013), (8) Durod-Azna (Shakerardakani et al. 2015), (9) Sargaz (Ghasemi et al. 2002), (10) Hasansalaran (Azizi et al. 2017), (11) Moro (Mohammadi et al. 2019), (12) Pir-Eshagh (Jamei et al. 2021), and (13) this study (SLUG).

The study area, located between Naqadeh and Miandoad towns in the West Azerbaijan province of NW Iran, consists mainly of sedimentary and igneous rocks (Fig 3). The igneous rocks are composed of volcanic rocks (Mahabad rhyolite with Precambrian age and Almalu basic lavas with Quaternary age), plutonic rocks (Khalifan granite with Late Carboniferous age and Pasveh granite with Upper Cretaceous-Eocene age). The Paleozoic sedimentation in the region has largely occurred during the Cambrian and the Permian. Stratigraphically, there is a distinct sedimentation gap during Ordovician-Carboniferous time in the study area. The Permian rocks comprise quartz sandstone and dolomitic limestone with a thin interlayer of lateritic bauxite. There are several small and single granite plutons (<1 km^2) with reddish pink in color and close to Qarah-Dagh and Tang-Balgeh villages (henceforward referred to as the South of Lake Urmia (SLU) granite). The SLU granite is non-conformably overlain by the Permian sequences (Fig 4a, b), which implies the occurrence of Late Paleozoic magmatism in the region.

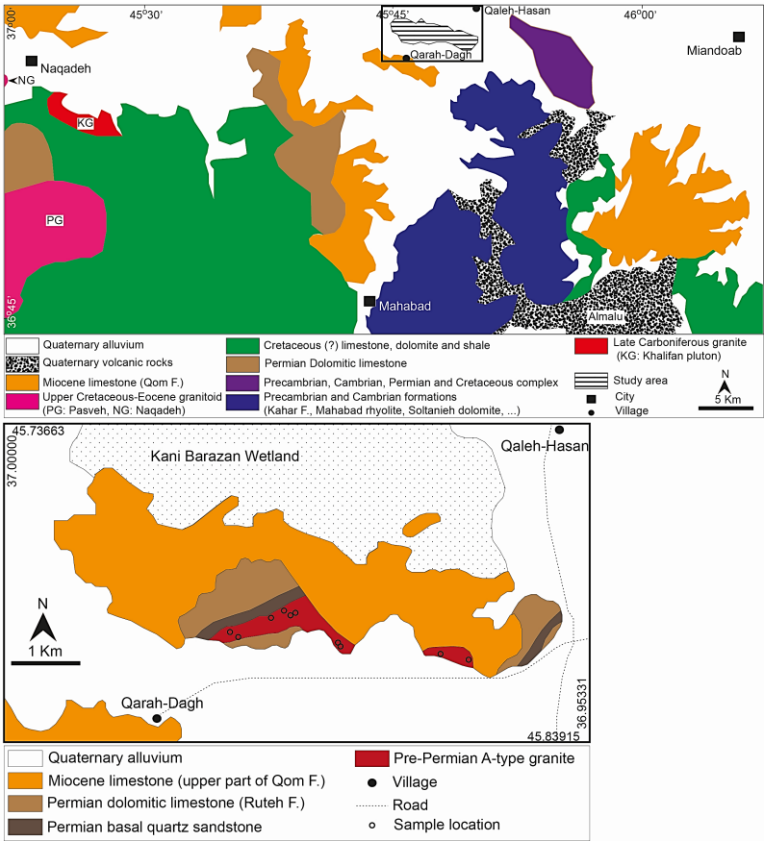

Fig 3 Geological map of the South Lake Urmia region (the above figure; modified after Eftekharnejad 1973), on which the A-type granite of Khalifan (Bea et al. 2011) and the Naqadeh and Pasveh granitoids (Mazhari et al. 2009a,b) are also shown. The below figure shows the geological map of the studied area in details modified after (Eftekharnejad 1980).

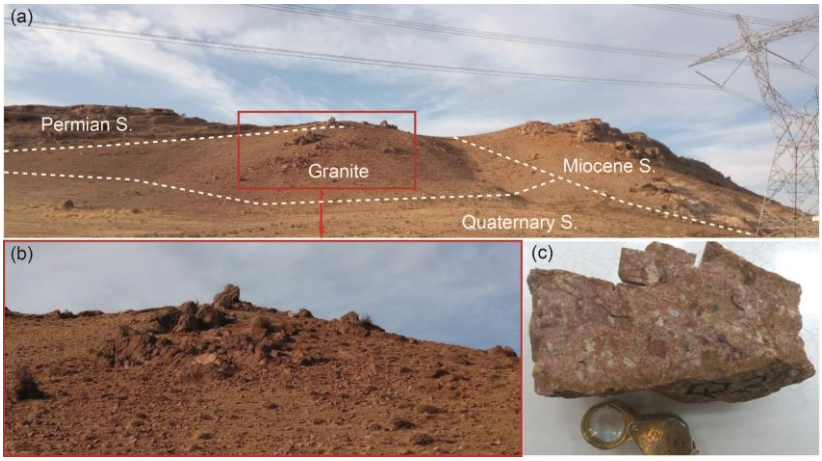

Fig 4 Field photographs of the SLU granite: (a) stratigraphic contacts of the granite with Permian, Miocene, and Quaternary sediments; (b) close-up view of the granite; (c) the granite hand specimen with distinct feldspar and Quartz crystals.

Eftekharnejad (1973) reported Pre-Permian age for the SLU granite and Post-Cretaceous age for the Khalifan granite, which occurred in the vicinity of the SLU granite. However, Bea et al. (2011) reported Late Carboniferous age (315±2 Ma) for the Khalifan A-type granite. Against the SLU granite, the Khalifan granite has a well-developed metamorphic aureole (Bea et al. 2011) with the Cretaceous country rocks (Eftekharnejad 1973, 1980). The Naqadeh and Pasveh granitoids (ca. 40-100 Ma) have also a metamorphic aureole similar to the Khalifan granite (Mazhari et al. 2009a, b). According to Bea et al. (2011), the recent plutons intruded unfossiliferous limestones, sandstones and claystones with an unknown age. However, the host rocks of the

plutons have been attributed to the Cretaceous by similarities to other Cretaceous sediments having paleontological evidence in the adjacent region (Eftekharnejad 1973, 1980; Khodabandeh and Soltani 2004). The Ghushchi granite (ca. 320 Ma), as the Late Paleozoic pluton occurred in the neighborhood of the SLU granite, is also non-conformably overlain by Permian sediments (Shafaii Moghadam et al. 2015). Therefore, the SLU granite can be more investigated for revealing the magmatic features of Late Paleozoic and determining the northeast precise boundary of the SSMMZ with the Central Iran.

3. Materials and methods

Thirteen rock samples with the slight alteration from the SLU granite were collected. The locations of studied samples are shown on the geological map (Fig 3). The samples were prepared for thin section studies by the optical microscopy. After petrographic studies, proper samples were selected for mineral and whole-rock chemical analyses.

Some mineral phases, such as biotite, plagioclase, and alkali-feldspar on the uncoated thin sections, were analyzed at the Kansaran Binaloud Company lab (Iran), with an X-Ray Probe Micro Analyzer (XPMA, Horiba XGT-7200) operating at a voltage of 50 kV and a beam current of 1 mA, and 100 μm probe diameter. The representative analyses are listed in Table 1. For major element analysis, whole-rock powders of five representative samples were fused with $Li_2B_4O_7$ and analyzed on fused discs by an X-ray fluorescence spectrometer (XRF) at the Kansaran Binaloud Company lab. Trace elements, including rare-earth elements (REE), were determined by an inductively coupled plasma-mass spectrometer (ICP-MS) using the Four-acid digestion method with uncertainties at 95% confidence level at the same lab. The detection limit for trace elements is 0.01-1 ppm. The analytical results for the samples are presented in Table 2.

Table 1. Representative XPMA analysis of some minerals from the SLU granite

Mineral	plagioclase					alkali-feldspar					biotite		
Point no.	1	2	3	4	5	1	2	3	4	5	1	2	3
Wt. %													
SiO_2	72.58	72.26	72.65	73.08	71.43	65.28	67.98	64.55	65.18	64.34	39.44	54.86	59.47
Al_2O_3	15.16	17.09	17.6	17.7	17.16	15.72	16.16	14.73	14.82	14.78	11.63	9.17	8.76
Fe_2O_3	0.87	0.69	0.27	0.22	1.23	0.46	0.36	0.32	0.32	0.48	35.06	26.25	25.68
MnO	n.d.	n.d.	n.d.	n.d.	n.d.	n.d.	n.d.	n.d.	n.d.	n.d.	0.51	0.36	0.33
MgO	n.d.	n.d.	n.d.	n.d.	n.d.	n.d.	n.d.	n.d.	n.d.	n.d.	4.32	3.06	3.06
CaO	1.23	1.57	1.5	1.47	2.56	2.15	2.28	2.19	2.06	1.81	7.79	5.34	1.68
Na_2O	9.77	7.75	7.4	7.02	7.13	2.3	1.04	1.83	0.62	3.25	n.d.	n.d.	n.d.
K_2O	0.39	0.64	0.58	0.51	0.49	14.08	12.17	16.38	17.01	15.34	1.05	0.86	0.9
Total	100	100	100	100	100	99.99	99.99	100	100.01	100	99.8	99.9	99.88

4. Petrography and mineral chemistry

The SLU pluton is characterized by almost homogenous rocks with medium to coarse crystals (Fig 4c). The appearance of rocks is pinkish to brownish and roughly without mafic minerals (leucocratic rocks). They show slightly dynamic metamorphism features, associated somewhat with shear structure and mylonitic fabric. Under the microscope, the rock forming minerals are alkali-feldspar (mostly microperthite up to 80%), quartz (up to 50%), plagioclase (minor up to 10%), biotite (up to 2%), apatite, zircon, Fe-Ti oxides, sericite, calcite, and clay minerals (Fig 5a, b, e). According to the recommendations of the International Union of Geological Sciences (IUGS) (Le Maitre et al. 2002), rock compositions for the SLU pluton range from quartz-alkali-syenite to alkali-granite. Alkali-feldspar is characterized by large subhedral to anhedral crystals having undoluse extinction and occasionally surrounded by fine-grained quartz crystals, which is depicted as a mylonitic fabric for the SLU pluton (Fig 5d). Quartz mostly occurs as coarse anhedral grains with undulose extinction. Micrographic texture, intergrowth of quartz and alkali-feldspar, is common in the studied rocks (Fig 5c). Plagioclase appears as small, subhedral, and individual crystals (Fig 5f).

Biotite, as the only mafic mineral, is rare and occurs as tiny tabular and subhedral crystals (Fig 5g). Chemically, alkali-feldspars are K-rich with $Ab_{5-23}An_{7-12}Or_{70-86}$, whereas plagioclases are Na-rich with $Ab_{80-91}An_{6-16}Or_{2-5}$ (Fig 6). The composition of observed biotite is Fe-rich and Al-poor (Table 1).

The SLU pluton can also be classified as alaskite/leucogranite, considering the modal abundance of K-feldspar and quartz (>90%), minor albite and scarce biotite.

Table 2. Representative whole rock analysis of the SLU granite

Sample no.	Q-2	Q-3	Q-6	Q-10	Q-13
Oxide (wt.%)					
SiO_2	77.98	78.46	78.83	75.8	77.75
TiO_2	0.105	0.123	0.112	0.139	0.178
Al_2O_3	11.59	11.88	11.35	13.08	11.44
$Fe_2O_3^t$	1.84	1.34	1.17	1.37	2.09
MnO	0.005	0.001	0.001	0.002	0.001
MgO	0.01	0.01	0.01	0.01	0.01
CaO	0.07	0.14	0.6	0.24	0.19
Na_2O	1.63	1.88	1.63	1.8	1.69
K_2O	5.6	4.84	5.02	6.57	4.88
P_2O_5	0.018	0.008	0.007	0.007	0.023
LOI	0.89	0.97	1.1	0.83	1.5
Total	99.74	99.65	99.83	99.85	99.75
Element (ppm)					
S (25)	56	149	100	92	63
Ba (0.1)	206.1	171.7	159.4	273.8	227.2
Rb (0.01)	132.16	110.91	114.91	164.18	89.33
Sr (0.5)	25.3	21.1	18.8	19.2	30.7
Y (0.1)	29.2	33.8	34.7	28.5	45.1
Zr (1)	47	90	59	44	62
Nb (0.01)	33.69	34.45	27.76	37.33	38.45
Th (0.01)	17.58	22.58	19.05	22.83	19.77
Pb (0.01)	19.09	13.83	12.78	30.27	18.62
Zn (0.1)	33	27	16	26	41
Cu (0.1)	41	150	141	98	29
Ni (1)	4	2	2	2	4
V (1)	6	4	2	4	5
Cr (1)	8	1	2	1	11
Hf (0.01)	2.51	4.42	2.71	2.45	2.43
Cs (0.01)	1	0.92	0.85	1.02	2.07
Ta (0.01)	2.64	2.81	2.01	2.42	2.23
Co (0.01)	0.1	0.2	0.2	0.1	0.4
U (0.01)	2.73	3.8	2.87	2.47	2.86
W (0.01)	0.76	0.76	0.67	0.83	1.12
Sn (0.01)	1.95	1.92	2.58	1.66	2.76
Mo (0.01)	1.3	1.2	0.8	1.9	1.7
La (0.01)	37.39	55.07	44.51	60.24	72.8
Ce (0.01)	76.21	107.09	91.08	113.83	135.43
Pr (0.01)	9.96	13.9	11.84	14.57	17.25
Nd (0.01)	44.67	64.15	54.4	67.23	81.22
Sm (0.01)	7.28	9.85	8.74	9.98	11.82
Eu (0.01)	1.62	1.72	1.55	1.6	1.89
Gd (0.01)	7.83	10.13	9.28	10.32	12.87
Tb (0.01)	1.23	1.54	1.13	1.29	1.47
Dy (0.01)	5.43	5.92	5.58	5.35	7.08
Ho (0.01)	1.02	1.12	1	0.99	1.28
Er (0.01)	2.95	3.39	2.93	2.7	3.63
Tm (0.01)	0.47	0.57	0.47	0.41	0.51
Yb (0.01)	3.32	4.31	3.39	3.01	3.47
Lu (0.01)	0.51	0.69	0.5	0.45	0.54
Ag (0.01)	0.38	0.54	0.36	0.39	0.33
As (1)	4	3	5	5	5
Be (0.01)	4.1	6.5	6.1	18.1	3.6
Bi (0.01)	0.08	0.05	0.04	0.04	0.04
Cd (0.01)	0.16	0.16	0.1	0.17	0.1
In (0.01)	0.32	0.32	0.34	0.32	0.36
Li (1)	4	4	3	5	4
Sb (0.01)	7.3	3.78	2.13	11.59	7.44
Sc (0.5)	1.4	1.8	1.2	1.6	2.5
Te (0.01)	0.23	0.15	0.11	0.45	0.25
Tl (0.01)	0.77	0.65	0.63	0.94	0.56
Eu/Eu^*	0.66	0.53	0.53	0.48	0.47
$(La/Sm)_N$	3.23	3.52	3.20	3.80	3.87
$(La/Yb)_N$	7.59	8.61	8.85	13.49	14.14
$(Tb/Yb)_N$	1.63	1.58	1.47	1.89	1.87
ASI	1.31	1.39	1.23	1.25	1.37

Abbreviation: LOI, loss on ignition; $Fe_2O_3^t$, total iron as Fe_2O_3; $Eu/Eu^* = Eu_N/\sqrt{(Sm)_N*(Gd)_N}$; ASI=Al/(Ca-1.67P+Na+K) as molecular. The detection limit of elements is presented in parenthesis and normalizing values are from Boynton (1984).

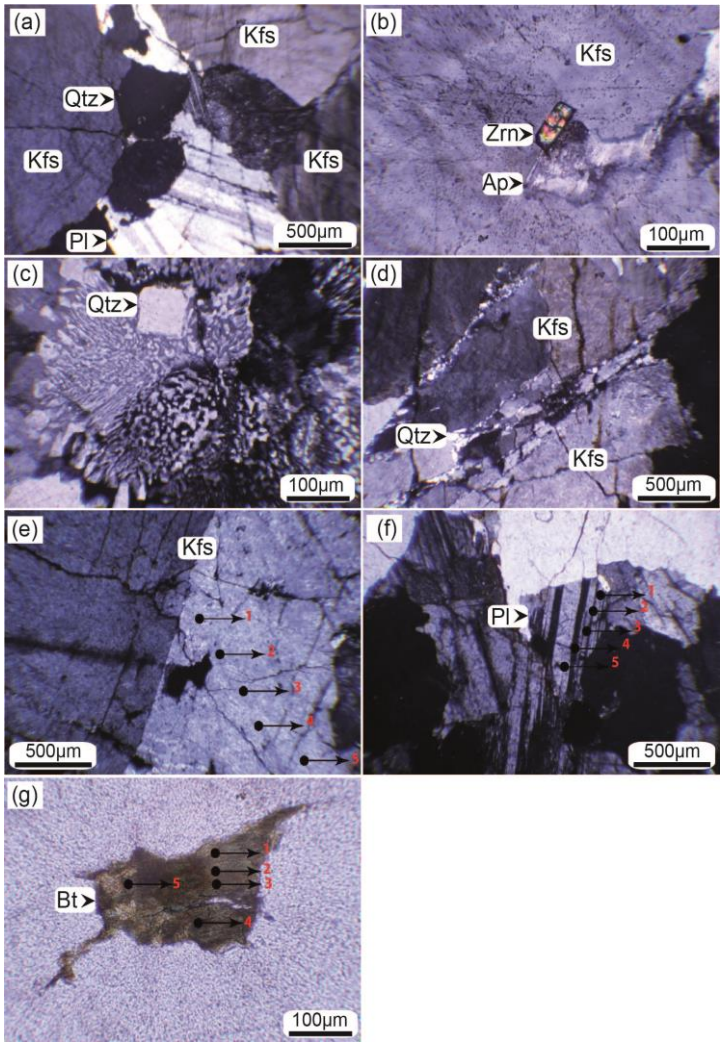

Fig 5 Microphotographs of the SLU granite: (a) alkali-feldspar (Kfs), quartz (Qtz), and plagioclase (Pl) as the main minerals of the granite with general granular texture; (b) Zircon (Zrn) and apatite (Ap) within alkali-feldspar; (c) micrographic texture; (d) mylonitic fabric with fine quartz grains around coarse alkali-feldspar crystals; (e) Carlsbad twining of alkali-feldspar with the points of analyzed by XPMA; (f) lamellar twining of plagioclase with the analyzed points (g) scarce biotite (Bt) with the location of analyzed points.

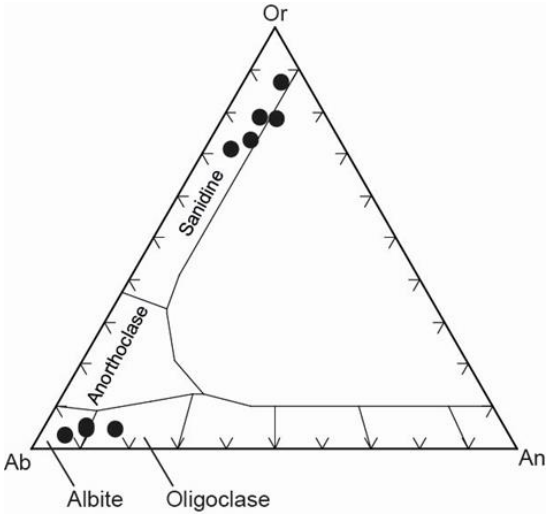

Fig 6 Feldspars composition plotted in the Or-Ab-An ternary (Deer et al. 1992).

5. Whole-rock geochemistry

5.1. Classification and tectonic setting

The SLU pluton has a relatively consistent composition with ~75 to ~78 wt.% SiO_2 and ~11 to ~13 wt.% Al_2O_3, corresponding to almost the same petrographic features of the rocks. Also, it has 4.84-6.57 wt.% K_2O, 0.07-0.6 wt.% CaO, and 0.83-1.5 wt.% LOI (Table 2). Based on the total alkalis (Na_2O+K_2O) wt.% vs. SiO_2 wt.% (TAS) nomenclature diagram (Middlemost 1994), the SLU pluton mostly consists of granite (Fig 7a). On the SiO_2 vs. $FeO^t/(FeO^t+MgO)$ discrimination diagram (Frost et al. 2001), the SLU pluton plots in the ferroan field, which is a chemical characteristic of A-type granites (Fig 7b).

The aluminum-saturation index (ASI) is defined as molecular Al/(Ca-1.67P+Na+K) and separates rocks into metaluminous (ASI < 1) and peraluminous (ASI > 1) varieties (Frost et al. 2001; Frost and Frost 2008). Plot of the samples in the ASI vs. Al/Na+K (A/NK) diagram (Fig 7c) show that all of the samples are peraluminous (ASI > 1, Na+K<Al). The potassium-rich nature of the studied rocks is characterized by the Ta/Yb vs. Ce/Yb diagram (Pearce 1983), as they plot in the shoshonitic field (Fig 7d).

Several chemical classifications for granitic series have been proposed (e.g., Whalen et al. 1987; Barbarin 1999; Frost et al. 2001).

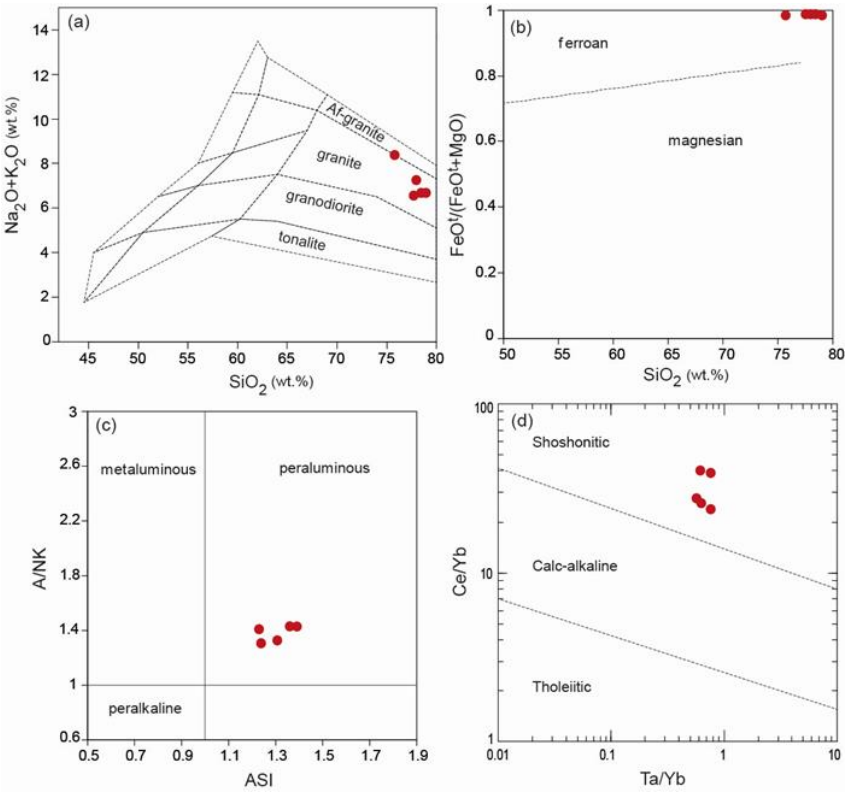

Fig 7 Chemical classification of the studied rocks: (a) Na_2O+K_2O vs. SiO_2 (TAS) nomenclature diagram (Middlemost 1994); (b) SiO_2 vs. $FeO^t/(FeO^t+MgO)$ discrimination diagram (Frost et al. 2001) showing the ferroan affinity for the studied granite; (c) ASI vs. Al/Na+K (A/NK) diagram (Frost et al. 2001) indicating the peraluminous nature for the studied rocks; (d) the shoshonitic feature of the SLU granite in the Ta/Yb vs. Ce/Yb diagram (Pearce 1983).

A-type affinity for the SLU granite is obtained from the FeO^t/MgO vs. Zr+Nb+Ce+Y (ppm) discrimination diagram (Fig 8a). Also, in the $(K_2O+Na_2O)/CaO$ vs. Zr+Nb+Ce+Y (ppm) diagram (Whalen et al. 1987), the samples mostly fall in the A-type field (Fig 8c). Dall'Agnol and Oliveira (2007) proposed the $FeO^t/(FeO^t+MgO)$ vs. Al_2O_3 diagram to distinguish oxidized and reduced A-type and calc-alkaline granites. In this diagram, the samples fall in the reduced A-type field (Fig 8b). On the Rb vs. Y+Nb tectonic discrimination diagram (Pearce et al. 1984; Pearce 1996), the samples plot inside the WPG (within-plate granite) and Post-COLG (post-collision granite) fields, but close to the WPG-VAG boundary (Fig 8d). Based on the trace element abundances, Eby (1990, 1992) divided A-type granites into two subgroups (A_1 and A_2). A_1 granites are linked with intraplate settings or continental rifts, while A_2 granites are commonly connected with post-collisional extension. The SLU granite displays chemical characters of the A_1 subgroup (Fig 9a-d) with relatively low Y/Nb ratios.

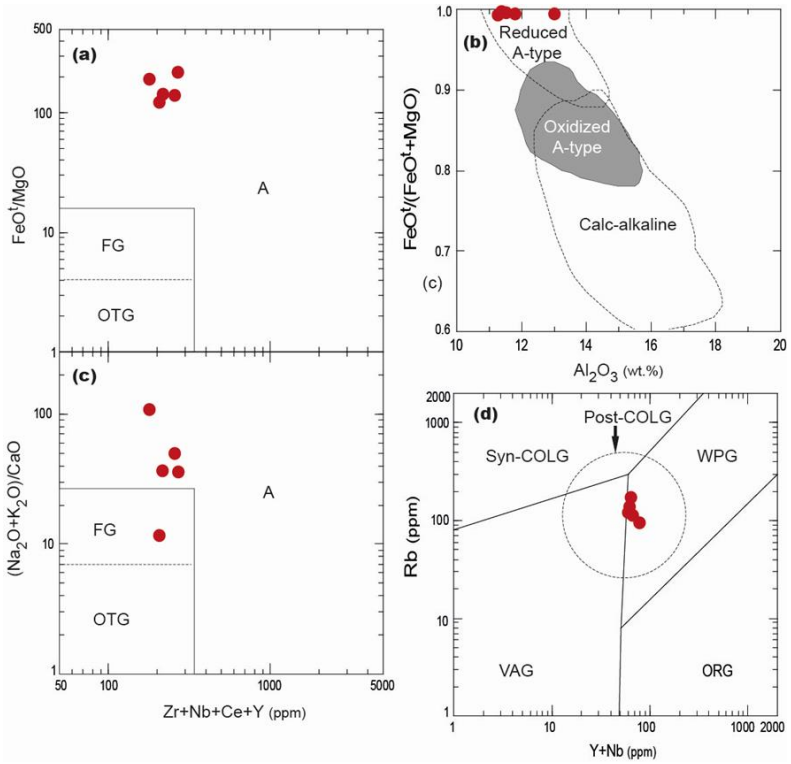

Fig 8 Granitoid type and tectonic setting of the studied granite: (a) FeO^t/MgO vs. Zr+Nb+Ce+Y diagram (Whalen et al. 1987); (b) FeO^t/(FeO^t+MgO) vs. Al_2O_3 diagram (Dall'Agnol and Oliveira 2007) showing the character of reduced A-type granites for the studied samples; (c) (K_2O+Na_2O)/CaO vs. Zr+Nb+Ce+Y diagram (Whalen et al. 1987) in which the SLU granite samples mostly fall in the A-type granite field; (d) Rb vs. Y+Nb diagram (Pearce et al. 1984; Pearce 1996), the samples plot inside the WPG and Post-COLG fields. Abbreviations: A, A-type granite; FG, fractionated felsic granites; OTG, unfractionated I-, M- and S-type granite; ORG, oceanic ridge granite; VAG, volcanic arc granite; Syn-COLG, syn-collision granite; Post-COLG, post-collision granite; WPG, within plate granite.

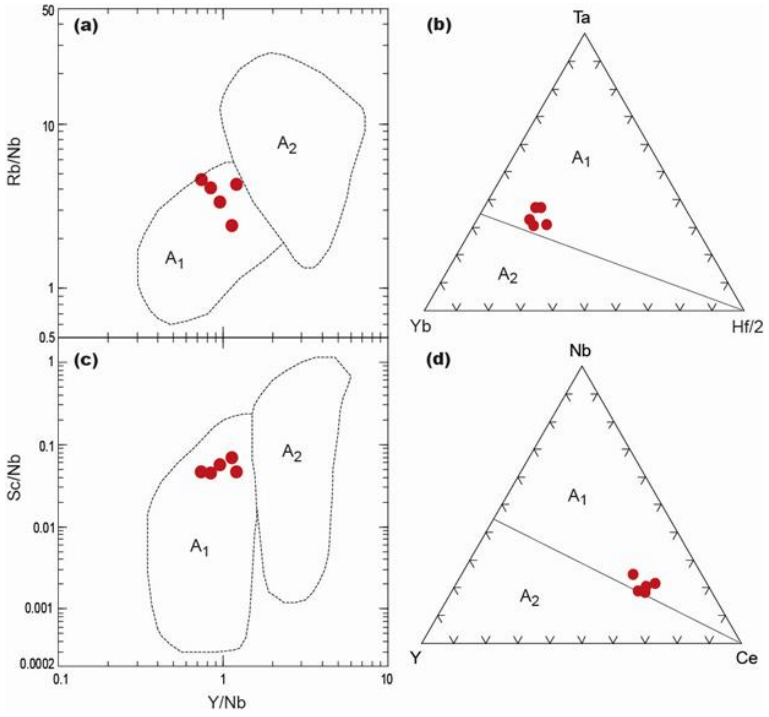

Fig 9 Discrimination of A_1 and A_2 subtype granites (Eby 1992): (a) Y/Nb vs. Rb/Nb diagram; (b) Ta-Yb-Hf/2 triangular diagram; (c) Y/Nb vs. Sc/Nb diagram; (d) Nb-Y-Ce triangular diagram. All of the samples fall within the field of A_1 subgroup.

5.2. Multi-element and REE patterns

Incompatible trace element concentrations normalized against N-MORB (Sun and McDonough 1989) are plotted in Fig 10a, indicating similar patterns for the samples. These patterns are characterized by significant enrichments in some incompatible elements such as Rb,Th, U, K, and Pb relative to Cs, Ba, Nb, Sr, P, Zr, and Ti. The samples exhibit strong negative anomalies in Sr, P, and Ti and positive anomalies for Pb. The Chondrite-normalized rare earth element (REE) patterns are illustrated in Fig 10b. They are LREE-enriched relative to the HREE with substantial negative Eu anomalies. The Eu/Eu*, [Eu/Eu*=$Eu_N/\sqrt{(Sm)_N*(Gd)_N}$)] ratio varies from 0.47 to 0.66 and the $(La/Yb)_N$, $(La/Sm)_N$, and $(Tb/Yb)_N$ ratios are 7.59-14.14, 3.20-3.87, and 1.47-1.89, respectively. The HREE from Ho to Lu displays nearly a flat pattern. Comparison of the multi-element and REE patterns of the SLU granite with those of some typical Late Paleozoic A-type granites, such as the Ghushchi, Hasanrobat, and Khalifan granites, show high resemblance (Fig 10a, b).

6. Discussion

6.1. Petrogenesis

The mineralogical and chemical features of the SLU granite, such as the existence of iron-rich mafic silicate (Fe-rich biotite) associated with microperthitic feldspar and Na-plagioclase (An<15), higher total alkalis and lower CaO, high FeO^t/MgO, negative Sr, P, Ti and Eu anomalies, and Y+Nb>50 ppm, are comparable with those of A-type granitoids formed in within-plate settings (Pearce et al. 1984; Whalen et al. 1987, 1996; Bonin 2007).

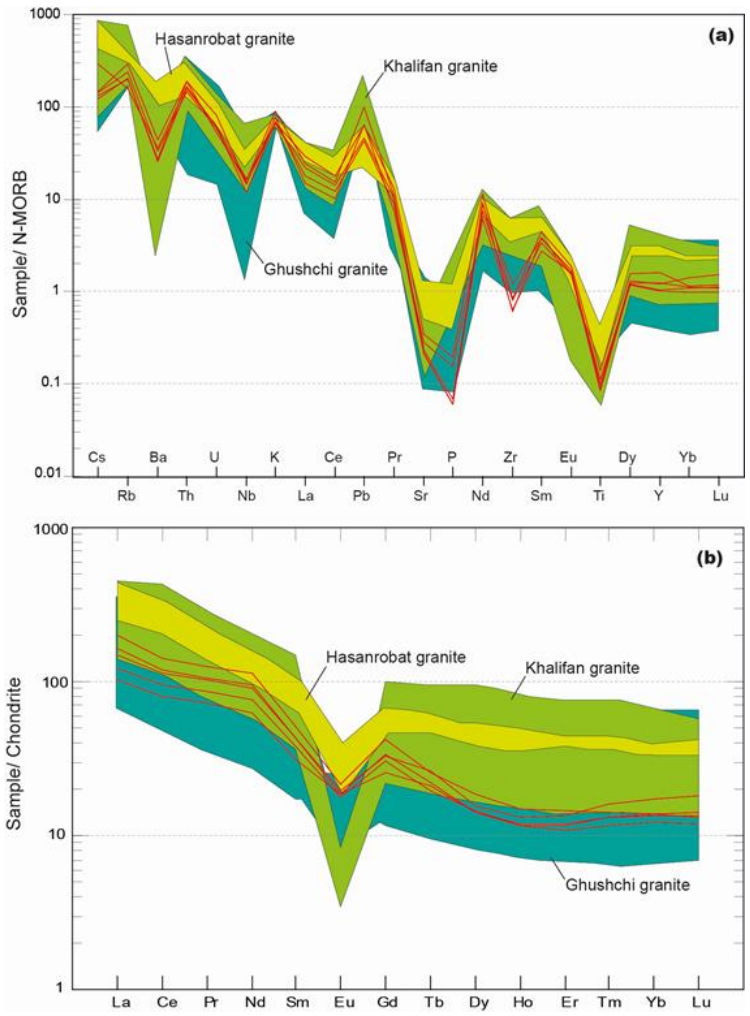

Fig 10 Geochemical comparison of the SLU granite (red lines) with some of the Late Paleozoic A-type granites in the multi-element normalized diagrams (comparison data are from Bea et al. (2011) (the Khalifan granite), Alirezaei and Hassanzadeh (2012) (the Hasanrobat granite), Shafaii Moghadam et al. (2015) (the Ghushchi granite)): (a) N-MORB-normalized multi-element patterns (normalizing data from Sun and McDonough 1989); (b) Chondrite-normalized rare earth element (REE) patterns (normalizing values from Boynton 1984).

Existing petrogenetic models for A-type granites comprise (1) partial melting of lower crustal granulite (Collins et al. 1982); (2) derivation from mantle-derived mafic and intermediate magmas (Bonin and Giret 1990; Turner et al. 1992); (3) involvement of mixed OIB-crust sources (Eby 1990, 1992); (4) melting of meta-igneous composition (Creaser et al. 1991); and (5) melting of alkali-metasomatized composition (Martin 2006). In the Nb-Y-Ce and Ta-Yb-Hf/2 triangular diagrams, as well the Y/Nb vs. Sc/Nb, and Y/Nb vs. Rb/Nb diagrams (Fig 9), all of the samples fall within the field of A_1-type granites, which are interpreted as fractional crystallization products of OIB-like mafic melts associated with intraplate settings or continental rifts. In contrast, A_2-type granites are partial melting products of juvenile continental crust and are commonly associated with collisional or post-collisional settings (Eby 1990, 1992).

Also, in the Y/Nb vs. Ce/Nb and Y/Nb vs. Yb/Ta plots (Fig 11a, c), the samples fall near or within the OIB field, suggesting the involvement of both mantle and crustal material in the petrogenesis of the SLU granite. In the Ta/Yb vs. Th/Yb diagram (Pearce 1983), the SLU granite along with the neighboring A-type granites (the Ghushchi and Khalifan granites) do not follow the mantle array, pointing to either derivation from an enriched mantle source to which an earlier subduction component had been added, or coupled crustal contamination with fractional crystallization, or both (Fig 11b). However, the SLU granite, along with some of the Late Paleozoic A-type rocks (Jamei et al. 2021), shows enrichment in the source, as they are plotted in the Zr/Y vs. Nb/Y diagram (Fitton et al. 1997) within the field of magmas derived from enriched sources (OIB or E-MORB) (Fig 11d). Based on the La/Yb vs. La and La/Sm vs. La diagrams (Fig 12a, b), the SLU A-type granite similar to the Khalifan and Hasanrobat granites follows the trend of fractional crystallization instead of partial melting processes. A similar trend (not shown) was achieved for the Ghushchi igneous complex (Shafaii Moghadam et al. 2015), where mafic and felsic rocks of the pluton were plotted. The distinct negative Ba, Sr, and Eu anomalies in the SLU granite suggest an important role for feldspar during partial melting and/or fractionation. The flat HREE patterns ($Tb_N/Yb_N \approx 1.4$-1.8) point to the absence of garnet in the magma source (Henderson 1989; Rollinson 1993).

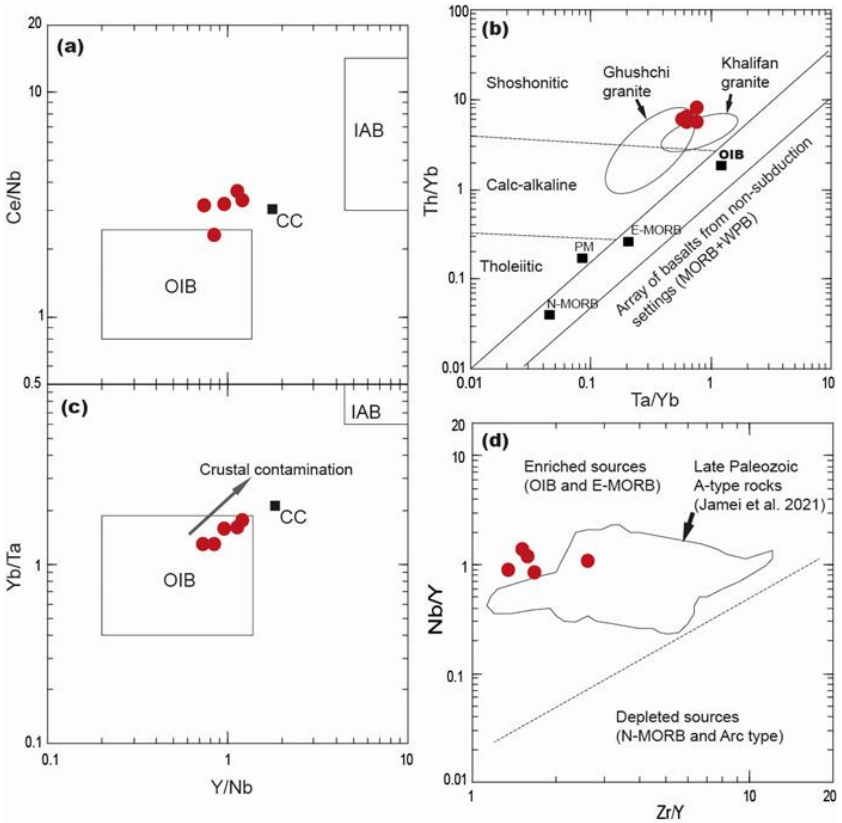

Fig 11 (a) Y/Nb vs. Ce/Nb diagram with the Oceanic Island Basalt (OIB) and Island Arc Basalt (IAB) fields (Eby 1990, 1992); (b) Ta/Yb vs. Th/Yb diagram (Pearce 1983) in which the SLU samples plotted close to the neighboring A-type granites field (Bea et al. 2011; Shafaii Moghadam et al. 2015), all pointing to the existence of crustal components; (c) Y/Nb vs. Yb/Ta plots (Eby 1992) (Continental Crust (CC) composition from Taylor and McLennan 1995) showing the compositional similarity of the samples with OIB associated with the involvement of crustal material in the genesis; (d) Zr/Y vs. Nb/Y diagram (Fitton et al. 1997) show that the SLU granite similar to the Late Paleozoic A-type rocks (Jamei et al. 2021) produced from an enriched source (plume type).

The positive Pb, U, and Th anomalies of the SLU granite may reflect the involvement of possible crustal contamination and more evolved residual melts in the genesis (Rollinson 1993). Nb depletion of the granite can be explained by fractionation of Nb-rich phases such as amphibole, titanite and rutile. The negative P, Ti, and Zr anomalies can be attributed to the fractionation of apatite, Fe-Ti oxides, and titanite, respectively, in the source. Zircon saturation geothermometry (Watson and Harrison 1983) shows temperatures of 702-769 °C for the SLU granite. These temperatures (T_{Zr}) were compared with those of the Khalifan and Hasanrobat granites, which are characterized by 820-900 °C and 834-880 °C, respectively (Fig 12c). All of the T_{Zr} plot in the temperature range of A-type granites. The mineralogical and geochemical characters of the SLU rocks show that they are relatively high fractionated than the Khalifan and Hasanrobat granites. Therefore, T_{Zr} for the SLU granite could be a minimum estimate of temperature of the initially emplaced magma, whereas that for the Khalifan and Hasanrobat granites may suggest a minimum estimate for magma temperature at a time before extensive crystallization (Miller et al. 2003). Comparing the maximum T_{Zr} for the A-type granitoids with various geoenvironment geotherms shows that the required melting temperatures are not normally achieved in the crust. Hence, mantle-derived mafic magmas providing heat and/or materials seem essential in the generation of the A-type granitoid melts (Eby 2011). Sr/Y ratios have been used to estimate the mean pressure in which the magmas were generated (Kay and Mpodozis 2002; Chapman et al. 2015). At low pressures, plagioclase has a high affinity for Sr, while Y is more incompatible. In contrast, Sr tends to enter the melting phase as an incompatible element, and Y wants to enter garnet and amphibole at high pressures (>12 kb) (Lee et al. 2007; Deng et al. 2018). The SLU granite has very low Sr (<31 ppm) and relatively high Y (~28–45 ppm); thus it is characterized by low Sr/Y ratios (0.54–0.87), suggesting that the melts generated at low pressures (<10 kb). The negative Eu and Sr anomalies and the flat HREE patterns indicate the fractional crystallization of plagioclase and further imply that the melts generated at a pressure <10 kb where plagioclase is stable and garnet is absent.

On the Nb/Ta vs. Zr/Hf diagram (Fig 12d), the studied rocks associated with the Khalifan and Hasanrobat A-type granites plot close to chondritic (or mantle) ratios, Nb/Ta = 17 and Zr/Hf = 40 (Eby 2004). However, there is a scatter towards lower ratios, especially Zr/Hf ratios, for the SLU and Khalifan granites. Titanite fractionation can lead to an increase Nb/Ta ratios (e.g., Green and Pearson 1987).

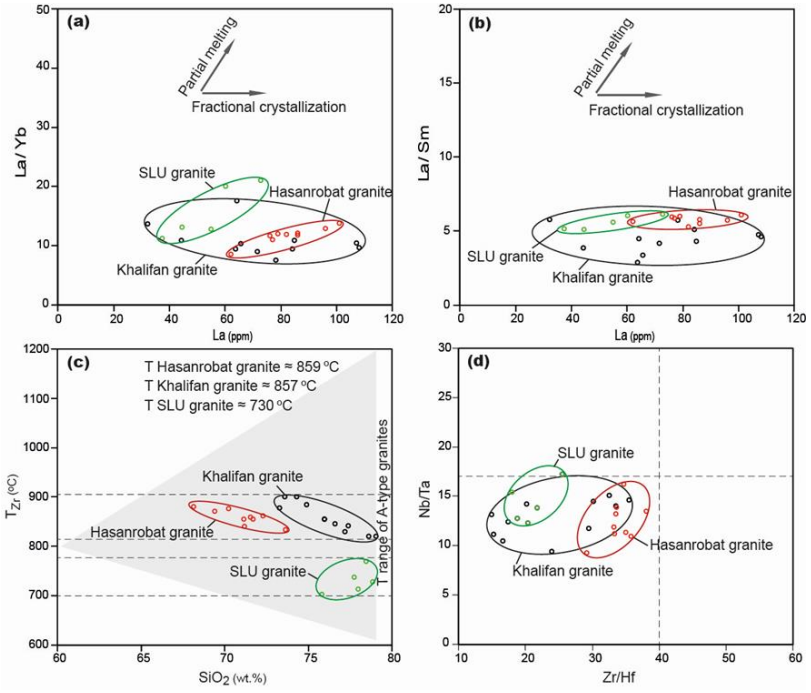

Fig 12 (a) La/Yb vs. La (b) La/Sm vs. La plots, showing the A-type granites (Khalifan, Hasanrobat and this study) mainly follow the fractional crystallization trend than the partial melting trend (the trends from Thirlwall et al. 1994); (c) T_{Zr} vs. SiO_2 plot for comparison of zircon saturation temperatures (Watson and Harrison 1983; $T_{Zr}=12900/[2.95+0.85M+\ln(496000/Zr_{melt})]$ with $M=[(Na+K+2*Ca)/(Al*Si)]$) from the three plutons (gray field, T_{Zr} range of A-type granitoids from Eby 2011); (d) Nb/Ta vs. Zr/Hf diagram for comparison of chondritic (or mantle) ratios in the three A-type granites.

Given the titanite/liquid partition coefficients for Nb and Ta, fractionation of this mineral leads to a decrease in the absolute Ta abundance and an increase in the Nb/Ta ratio (Green 1995; Eby 2004). Hence, relatively low Nb/Ta ratios in the studied rocks can be explained by fractionation of Nb-rich minerals such as amphibole and biotite instead of titanite. Zr/Hf ratio is generally constant during fractional crystallization; however, excessive fractionation could lead to enrichment in Hf than Zr (Mason and Moore 1982; Rollinson 1993). Therefore, the SLU granite is inferred to be a result of a high degree of fractional crystallization from mantle-derived melts. As a result, the scenario of the combined mantle and crustal sources for the origin of A-type granitoids is consistent with the features of SLU granite. The SLU granite has probably formed by fractional crystallization of an enriched mantle-derived parental mafic magma (OIB) with crustal interactions. The similar petrogenetic models have been proposed for the neighboring A-type granites such as the Ghushchi and Khalifan granites. Derivation from a sub-continental enriched mantle source suggested for the Ghushchi complex magmas, where there is a genetic relationship between mafic and felsic magmas; the granites exhibit the geochemical character of A-type magmas, whereas the gabbronorites have OIB-type signature (Shafaii Moghadam et al. 2015). Also, derivation from an infra-crustal source was suggested for the Khalifan granites (Bea et al. 2011). High temperatures in the source regions and the involvement of mafic magmas in the genesis of the A-type rocks would be best provided in a continental rift zone, where upwelling of the asthenosphere or lithospheric extension could be produced a high mantle heat flow and sub-continental enriched melts.

6.2. Geodynamic implications

Our data suggest that the SLU granite has the chemical composition of the within-plate A-type granites. Moreover, the SLU granite displays the features of the A_1 subgroup of A-type granites, providing a contribution of OIB-like mafic melts in the genesis. The OIB-like chemical affinities are somewhat preserved in the studied rocks in spite of their high fractionation. OIB magmas are commonly considered as a result of mantle plume activity (e.g., Weaver 1991). Hence, the most plausible process for the generation of the SLU granite is lithospheric extension, thinning of the lithosphere and upwelling of the asthenosphere. In paleogeographic and plate tectonic reconstructions, the Southern and Central structural units of Iran (Stocklin 1968; Berberian and King 1981) are considered part of the Cimmerian superterrane (Stampfli and Borel 2002). The individual fragments of the Cimmerian superterrane, such as the Sanandaj-Sirjan, Alborz, and Central Iran were detached from the northern/eastern of Gondwana during the Late Carboniferous-Early Permian as a consequence of the opening of Neotethys. These crustal fragments were accreted to the Variscan terranes (Laurasia) in the Middle Jurassic during the closure of Paleotethys (Stampfli and Borel 2002). The opening of Neotethys (Permotethys) was synchronous with the closure of Paleotethys during Permian and Triassic times (Sengör 1987; Stampfli et al. 1991). The time of the opening of Neotethys in Iran is discussed based on the combination of paleontological data with Carboniferous volcanism and tectonics (Saccani et al. 2013; Tavakoli-Shirazi et al. 2013; Shafaii Moghadam et al. 2015; Arefifard 2017). According to Arefifard (2017), in the Late Carboniferous, data from both smaller foraminifer and fusulinid assemblages in North and Central Iran reveal the similarity of these faunas with their northern Paleotethys counterparts. This can be inferred as a sign of the beginning of the separation of Iran from the northern margin of Gondwana and its movement towards the North. The Zagros suture is located along the discontinuous ophiolites at the southwestern margin of the SSMMZ (outer sub-zone in Fig 2). Based on the Zagros ophiolites and plutons of roughly the same age in the SSMMZ, subduction of Neotethys beneath the SSMMZ with a NE-dipping was initiated in the Middle to Late Triassic (e.g., Berberian and Berberian 1981; Dercourt et al. 1986; Agard et al. 2005; Verdel et al. 2011). Continuous subduction and arc magmatism during the Mesozoic was led to scattered Jurassic to Cretaceous plutons, mainly within the SSMMZ with features of calc-alkaline I-type granite (Berberian and Berberian 1981). Furthermore, the granitic plutons of SSMMZ vary in age from Neoproterozoic to Eocene and have S and I-type nature rather than A-type (e.g., Hassanzadeh et al. 2008; Mahmoudi et al. 2011; Alirezaei and Hassanzadeh 2012; Ahadnejad 2013). However, most plutons were formed during Jurassic-Paleocene times with I-type affinities (e.g., Berberian and Berberian 1981; Masoudi et al. 2002; Mohajjel et al. 2003; Shahbazi et al. 2010). The opening and closing processes of the Neotethys Ocean in Iran could be mainly traced in the SSMMZ (e.g., Berberian and King 1981; Alavi 1994; Mohajjel et al. 2003). The Paleozoic magmatism of SSMMZ, especially alkaline and/or A-type magmas, may provide good evidence of the timing of the Neotethys rifting. Clues of the early phases of the Neotethys opening in the SSMMZ during the Late Paleozoic are elongated in NW-SE direction, from NW Iran such as the Misho and Ghushchi magmatic complexes (e.g., Saccani et al. 2013; Shafaii Moghadam et al. 2015) to SE Iran such as the Sargaz-Abshour complex (Ghasemi et al. 2002). The U-Pb ages obtained from the Late Paleozoic felsic igneous rocks of Iran along with some mafic rocks, orthogneiss and amphibolites indicate that the rifting of the SSMMZ from northern Gondwana and the opening of the Neotethys Ocean was probably initiated in the Late Devonian (Jamei et al. 2021) to Early Carboniferous (Saccani et al. 2013). The present granitoid rocks generally have A-type affinities and occur as single or composite bodies, which are commonly sheared and mylonitized (Alirezaei and Hassanzadeh 2012). They are mainly emerged in the

northeast margin of the SSMMZ and around the structural depressions such as Lake Urmia, Meyghan, Gavkhouni, Sirjan, and Jaz Murian (Fig 2). The boundary of the SSMMZ with the UDMA to the northeast is characterized by a series of structural depressions formed by compression (Alavi 1994). According to Alavi (1994), the SSMMZ is characterized by large-scale composite duplex structures or low- and high-angle NE-dipping imbricate systems, which have transported numerous sheets of metamorphosed and non-metamorphosed Phanerozoic rocks for tens or possibly hundreds of kilometers since the Late Cretaceous. Therefore, the main outcrops of Late Paleozoic rocks, including the SLU granite, in the northeast margin of the SSMMZ could be related to the southwestward displacement of younger rocks by thrust faulting.

It is noted that thrusting and deformation in the SSMMZ climaxed in the Miocene because of the continental collision of Arabia and Central Iran following the opening of the Red Sea and the Gulf of Aden Mohajjel (et al. 2003). According to Stocklin (1968) and Berberian and King (1981), Iran formed from three major structural units/domains comprising the Southern domain (Zagros orogenic belt including SSMMZ), the Central domain (Central Iran ± Alborz belt), and the Northern domain (Kopeh-Dagh + Caspian depression ± Alborz belt). The Southern and Central domains have Gondwanan affinity based on flora/fauna and excellent correlation of Paleozoic facies with basins in Arabia or India (e.g., Ghavidel-Syooki 1995; Stampfli 2000; Arefifard 2017). Therefore, they are considered part of the Cimmerian superterrane. The SLU granite has the geochemical features of the A_1 subtype of A-type granitoids and provides evidence for extensional tectonics and rifting of the SSMMZ away from Gondwana during the Late Paleozoic. However, the Khalifan pluton, the neighboring Late Paleozoic A-type granite to the SLU granite, has been attributed to the Variscan terranes by Bea et al. (2011). Notwithstanding the absence of involvement of the Cimmerian terranes detached from Gondwanide terranes in the Variscan (Hercynian) orogeny (von Raumer et al. 2003) and generally the lack of major Variscan magmatic rocks in the Southern and Central domains, they suggested a derivation from the Variscan terranes of the Eurasian margin for this part of Iran.

The SLU granite is situated in NW Iran, a complex area where the three main Iranian structural zones are joined together and associated with the major old active faults, the Tabriz and Urmia faults. Therefore, in this area there are some complexities in the geological interpretations on the subject of Neotethys opening.

On the other hand, the Sanandaj-Sirjan block borders are controversial because the geological indications of Neotethys opening are rigorously affected by some younger processes; in a side, the border is concealed by the Paleogene intense magmatism (i.e., UDMA), and in another side, it is covered by multi-generation thrust faulting.

Nevertheless, the southwest boundary of SSMMZ is restricted to the Zagros Main thrust and the northeast border of SSMMZ is conventionally limited to the UDMA (e.g., Berberian and King 1981; Alavi 1994; Mohajjel et al. 2003; Alavi 2004). Considering the recent studies on the Late Paleozoic rocks from NW Iran, It seems that the late border could be extended to the major old active faults such as the right-lateral Tabriz, Qom-Zefreh, and Nain-Baft faults, as it is also suggested by Mehdipour Ghazi and Moazzen (2015). Overall, the present study as well as comparing the present data on the Late Paleozoic A-type rocks in the SSMMZ and NW Iran show that evidence for early stages of the Neotethys opening is mainly discovered in the northeast margin of SSMMZ and around the structural depressions (so-called ‘Mesozoic back-arc’ in McCall and Kidd (1982), ‘Tertiary fore-arc’ in Berberian (1983) and Alavi (1994), ‘inner sub-zone’ in Mohajjel et al. (2003), and ‘intra-arc basin’ in Shahabpour (2007; 2010)). Consequently, the Late Paleozoic A-type units, including the SLU granite, are distributed predominantly close to the old faults and the modern depressions. They are characterized primarily by the coeval bimodal magmatism with OIB-like affinity (e.g., Alirezaei and Hassanzadeh 2012; Saccani et al. 2013; Shakerardakani et al. 2015; Shafaii Moghadam et al. 2015; Azizi et al. 2017) and overlain by Permian to Early Mesozoic marine sediments, suggesting an extensional regime related to upwelling of mantle plume during the Late Paleozoic.

7. Conclusions

Based on the mineralogical and geochemical characters, the SLU granite is inferred to be the result of a high degree of fractional crystallization from an enriched mantle-derived parental mafic magma with crustal interactions. The granitic melts formed in low pressure (<10 kb), low temperature (e.g., $T_{Zr}\approx730$ °C), water-poor, and reduced conditions. The SLU granite shows ferroan, peraluminous, and shoshonitic affinities and the geochemical features of A-type granites.

Moreover, the SLU granite displays the features of the A_1 subgroup of A-type granites, providing a contribution of OIB-like mafic melts in the genesis within a probable extensional setting. Therefore, the SLU A-type granite similar to the Late Paleozoic A-type rocks, such as the Misho, Ghushchi, Hasanrobat, and Khalifan magmatic suites, could be as evidence for the early phases of Neotethys opening in Iran.

During the Neotethys opening, melting of sub-continental lithospheric mantle could be occurred by upwelling of the asthenosphere or extension of the lithosphere to produce primitive magmas (OIB-like). Extreme fractionation of the produced hot primitive mafic magmas was probably associated with crustal interactions to generate the dry parent granitic magmas of the SLU pluton. The Late Paleozoic A-type rocks that

occurred parallel to the Neotethys suture are mainly emerged in the northeast margin of the SSMMZ and around the structural depressions such as Lake Urmia, Meyghan and Sirjan, probably due to the southwestward displacement of younger rocks by thrust faulting since the Late Cretaceous to the present with a climax in the Miocene.

Acknowledgements

This work was financially supported by the Research Bureau of the Payame Noor University (Iran), for which we are thankful. The authors would like to acknowledge contributions of the IJES editors and reviewers, in improving the manuscript by providing constructive and thoughtful comments.

References

Advay M, Ghalamghash J (2011) Petrogenesis and U–Pb dating zircon of granites of Heris (NW of Shabestar), eastern Azerbaigan province, *Iranian Journal Crystallography Mineralogy* 4:633–648.

Advay M, Jahangiri A, Mojtahedi M, Ghalamghash J (2010) Petrology and geochemistry of Ghoshchi batholith, NW Iran, *Journal of Crystallography and Mineralogy* 17:716–733.

Agard P, Omrani J, Jolivet L, Mouthereau F (2005) Convergence history across Zagros (Iran): constraints from collisional and earlier deformation, *International Journal of Earth Sciences* 94:401–419.

Ahadnejad V (2013) Comparative review of the Northern Sanandaj-Sirjan Zone granitoids, *Journal of Tethys* 1:128–137.

Ahmadi Khalaji A, Esmaeily D, Valizadeh MV, Rahimpour-Bonab H (2007) Petrology and geochemistry of the granitoid complex of Boroujerd, Sanandaj-Sirjan Zone, Western Iran, *Journal of Asian Earth Sciences 2*9:859–877.

Alavi M (1991) Sedimentary and structural characteristics of the Paleo-Tethys remnants in northeastern Iran, *Geological Society of America Bulletin* 103:983–992.

Alavi M (1994) Tectonics of the Zagros Orogenic belt of Iran; new data and interpretations, *Tectonophysics* 299:211–238.

Alavi M (2004). Regional stratigraphy of the Zagros folded-thrust belt of Iran and its proforeland evolution, *Am J Sci* 304:1–20.

Aliani F, Maanijou M, Sabouri Z, Sepahi AA (2012) Petrology, geochemistry and geotectonic environment of the Alvand Intrusive Complex, Hamedan, Iran, *Chemie der Erde-Geochemistry* 72:363–383.

Alirezaei S, Hassanzadeh J (2012) Geochemistry and zircon geochronology of the Permian A-type Hasanrobat granite, Sanandaj–Sirjan belt: a new record of the Gondwana break-up in Iran, *Lithos* 151:122–134.

Arefifard S (2017) Foraminiferal - based paleobiogeographic reconstructions in the Carboniferous of Iran and its implications for the Neo-Tethys opening time: A synthesis, *Geologica Acta* 15:135–151.

Arvin M, Pan Y, Dargahi S, Malekizadeh A, Babaei A (2007) Petrochemistry of the Siah-Kuh granitoid stock southwest of Kerman, Iran: implications for initiation of Neotethys subduction, *Journal of Asian Earth Sciences* 30:474–489.

Asadpour M, Pourmoafi SM, Heuss S (2013) Geochemistry, petrology and U-Pb geochronology of Ghazan mafic-ultramafic intrusion, NW Iran, *Petrology* 4:1-16 (in Persian).

Azizi H, Chung SL, Tanaka T, Asahara Y (2011) Isotopic dating of the Khoy metamorphic complex (KMC), northwestern Iran: a significant revision of the formation age and magma source, *Precambrian Research* 185:87–94.

Azizi H, Kazemi T, Asahara Y (2017) A-type granitoid in Hasansalaran complex, northwestern Iran: Evidence for extensional tectonic regime in northern Gondwana in the Late Paleozoic, *Journal of Geodynamics* 108:56–72.

Azizi H, Moinevaziri H (2009) Review of the tectonic setting of Cretaceous to Quaternary volcanism in northwestern Iran, *Journal of Geodynamics* 47:167–179.

Barbarin B (1999) A review of the relationships between granitoid types, their origins and their geodynamic environments, *Lithos* 46:605–626.

Bea F, Mazhari A, Montero P, Amini S, Ghalamghash J (2011) Zircon dating, Sr and Nd isotopes, and element geochemistry of the Khalifan pluton, NW Iran: evidence for Variscan magmatism in a supposedly Cimmerian superterrane, *Journal of Asian Earth Sciences* 40:172–179.

Berberian F, Berberian M (1981) Tectono-Plutonic Episodes in Iran, In: Zagros, Hindu Kush, Himalaya Geodynamic Evolution, Geodynamic Series, *American Geophysical Union* 3:5-32.

Berberian M (1983) Generalized tectonic Map of Iran, Geological Survey of Iran, Report No. 52.

Berberian M, King GCP (1981) Towards a paleogeography and tectonic evolution of Iran, *Canadian Journal of Earth Sciences* 18:210–265.

Bonin B (2004) Do coeval mafic and felsic magmas in post-collisional to within-plate regimes necessarily imply two contrasting, mantle and crustal, sources? A review, *Lithos* 78:1–24.

Bonin B (2007) A-type granites and related rocks: evolution of a concept, problems and prospects, *Lithos* 97:1–29.

Bonin B, Giret A (1990) Plutonic alkaline series: Daly gap and intermediate compositions for liquids filling up crustal magma chambers, *Schweizerische Mineralogisch und Petrographische Mitteilungen* 70:175–187.

Boynton WV (1984) Geochemistry of rare earth elements: meteorite studies, In: Henderson, P. (Ed.),

Rare Earth Element Geochemistry, Elsevier, New York, pp. 63-114.

Chapman JB, Ducea MN, Decelles PG (2015) Tracking changes in crustal thickness during orogenic evolution with Sr/Y: an example from the North American Cordillera, *Geology* 43:919–922.

Chiu HY, Chung SL, Zarrinkoub MH, Mohammadi SS, Khatib MM, Iizuka Y (2013) Zircon U–Pb age constraints from Iran on the magmatic evolution related to Neotethyan subduction and Zagros orogeny, *Lithos* 162–163:70–87.

Coleman RG, DeBari S, Peterman Z (1992) A-type granite and the Red Sea opening, *Tectonophysics* 204:27–40.

Collins WJ, Beams SD, White AJR, Chappell BW (1982) Nature and origin of A-type granites with particular reference to southeastern Australia, *Contributions to Mineralogy and Petrology* 80:189–200.

Collins WJ, Huang HQ, Bowden P, Kemp AIS (2018) Repeated S–I–A-type granite trilogy in the Lachlan Orogen and geochemical contrasts with A-type granites in Nigeria: implications for petrogenesis and tectonic discrimination, in Janousek, V., Bonin, B., Collins, W.J., Farina, F. & Bowden, P. (eds) Post-Archean Granitic Rocks: Petrogenetic Processes and Tectonic Environments. Geological Society, London, Special Publications, 491.

Creaser RA, Price RC, Wormold RJ (1991) A-type granite revised: Assessment of residual source model, *Geology* 19:163-166.

Dall'Agnol R, de Oliveira DC (2007) Oxidized, Magnetite-Series, Rapakivi-Type Granites of Carajas, Brazil: Implications for Classification and Petrogenesis of A-Type Granites, *Lithos* 93:215–233.

Deer WA, Howie RA, Zussman J (1992) An introduction to the Rock Forming Minerals, 2nd ed. Longman Group Ltd, Harlow (712 pp).

Delavari M, Arab-Asadi F, Mohammadi A (2019) Paleozoic magmatism in the southwest of Julfa (northwestern Iran): Geochemical characteristics, U-Pb dating and tectonic setting, *Petrology* 38:99–120 (in Persian).

Deng C, Sun D, Sun G, Lv C, Qin Z, Ping X, Li G (2018) Age and geochemistry of Early Ordovician A-type granites in the Northeastern Songnen Block, NE China, *Acta Geochimica* 37:805-819.

Dercourt J, Zonenshain LP, Ricou LE, Kazmin VG, Le Picon X, Knipper AL, Grandjacquet C, Sbortshikov IM, Geyssany J, Lepverier C (1986) Geological evolution of the Tethys belt from the Atlantic to the Pamirs since the Lias, *Tectonophysics* 123:241–315.

Dokuz A, Uysal I, Kaliwoda M, Karsli O, Ottley CJ, Kandemir R (2011) Early abyssal and late SSZ-type vestiges of the Rheic oceanic mantle in the Variscan basement of the Sakarya Zone, NE Turkey: implications for the sense of subduction and opening of the Paleotethys, *Lithos* 127:176–191.

Eby GN (1990) The a-type granitoids: a review of their occurrence and chemical characteristics and speculations on their petrogenesis, *Lithos* 26:115–134.

Eby GN (1992) Chemical subdivision of the A-type granitoids: petrogenetic and tectonic Implications, *Geology* 20:641–644.

Eby GN (2004) Petrology, geochronology, mineralogy, and geochemistry of the Beemerville alkaline complex, northern New Jersey, In Puffer, J. H. and Volkert, R. A. (Eds.) Neoproterozoic, Paleozoic, and Mesozoic Intrusive Rocks of Northern New Jersey and Southeastern New York. Twenty-First Annual Meeting Geological Association of New Jersey, Mahwah, NJ, pp. 52-68.

Eby GN (2011) A-type granites: characteristics, petrogenesis and their contribution to the growth of the continental crust, VII Hutton Symposium on Granite and Related rocks, Avila, Spain.

Eftekharnejad J (1973) 1:250,000 Geological Map of Mahabad, Geological Survey of Iran Press.

Eftekharnejad J (1980) 1:100,000 Geological Map of Mahabad, Geological Survey of Iran Press.

Esna-Ashari A, Tiepolo M, Valizadeh MV, Hassanzadeh J, Sepahi AA (2012) Geochemistry and zircon U-Pb geochronology of Aligoodarz granitoid complex, Sanandaj-Sirjan zone, Iran, *Journal of Asian Earth Sciences* 43:11–22.

Fazlnia A, Moradian A, Rezaei K, Moazzen M, Alipour S (2007) Synchronous activity of anorthositic and S-type granitic magmas in Chah–Dozdan Batholith, Neyriz, Iran: evidence of zircon SHRIMP and monazite CHIME dating, *Iranian Journal of Sciences* 18:221–237.

Fazlnia A, Schenk V, van der Straaten F, Mirmohammadi M (2009) Petrology, geochemistry, and geochronology of trondhjemites from the Qori Complex, Neyriz, Iran, *Lithos* 112:413–433.

Fitton JG, Saunders AD, Norry MJ, Hardarson BS, Taylor RN (1997) Thermal and chemical Of the Iceland plume, *Earth and Planetary Science Letters* 153:197–208.

Frost BR, Arculus RJ, Barnes CG, Collins WJ, Ellis DJ, Frost CD (2001) A geochemical classification of granitic rocks, Journal of Petrology 42:2033–2048.

Frost BR, Frost CD (2008) A Geochemical Classification for Feldspathic Igneous Rocks, *Journal of Petrology* 49:1955-1969.

Frost CD, Frost BR (2011) On Ferroan (A-type) granitoids: their compositional variability and modes of origin, *Journal of Petrology* 52:39–53.

Ghaffari M, Rashidnejad-Omran N, Dabiri R, Chen B, Santos JF (2013) Mafic–intermediate plutonic rocks of the Salmas area, northwestern Iran: their source and petrogenesis significance. *International Geology Review* 55(16): 2016-2029.

Ghalamghash J, Nédélec A, Bellon H, Vousoughi Abedini M, Bouchez JL (2009) The Urumieh plutonic complex (NW Iran), a record of the geodynamic

evolution of the Sanandaj–Sirjan zone during Cretaceous times- part I: petrogenesis and K/Ar dating, *Journal of Asian Earth Sciences* 35:401–415.

Ghasemi H, Jutea T, Bellon H, Sabzehei M, Whitechurch H, Ricou LE (2002) The mafic-ultramafic complex of Sikhoran (Central Iran): A polygenetic ophiolite complex, *Comptes Rendus Geoscience* 334:431–438.

Ghavidel-Syooki M (1995) Palinostratigraphy and paleogeography of a Paleozoic sequence in the Hasankdar area, central Alborz range, northern Iran, *Review of Paleobotany and Palinology* 86:91–109.

Green TH (1995) Significance of Nb/Ta as an indicator of geochemical processes in the crust mantle system, *Chemical Geology* 120:347-359.

Green TH, Pearson NJ (1987) An experimental study of Nb and Ta partitioning between Ti-rich minerals and silicate liquids at high pressure and temperatures, *Geochimica et Cosmochimica Acta* 51:55-62.

Hassanzadeh J, Stockli DF, Horton BK, Axen GJ, Stockli LD, Grove M, Schmitt AK, Walker JD (2008) U–Pb zircon geochronology of late Neoproterozoic–Early Cambrian granitoids in Iran: implications for paleogeography, magmatism, and exhumation history of Iranian basement, *Tectonophysics* 451:71–96.

Henderson P (1989) Rare earth element geochemistry, Third edition, Elsevier 510 p.

Honarmand M, Li XH, Nabataian G, Neubauer F (2017) In-situ zircon U-Pb age and Hf-O isotopic constraints on the origin of the Hasan-Robat A-type granite from Sanandaj-Sirjan zone, Iran: Implications for reworking of Cadomain arc igneous rocks, *Mineralogy and Petrology* 111:659–675.

Jamei S, Ghorbani M, Williams IS, Moayyed M (2021) Tethyan oceans reconstructions with emphasis on the Early Carboniferous Pir-Eshagh A-type rhyolite and the Late Palaeozoic magmatism in Iran, *International Geology Review* 63:1389-1405.

Kay SM, Mpodozis C (2002) Central Andean ore deposits linked to evolving shallow subduction systems and thickening crust, GSA Today 11:4–11.

Khodabandeh AA, Soltani GA (2004) 1/100,000 Geological map of Naqadeh, Geological Survey of Iran Press.

Landenberger B, Collins WJ (1996) Derivation of A-type granites from a dehydrated charnockitic lower crust: evidence from the Chaelundi complex, eastern Australia, *Journal of Petrology* 37:145–170.

Le Maitre RW, Streckeisen A, Zanettin B, Le Bas MJ, Bonin B, Bateman P, Bellieni G, Dudek A, Efremova SA, Keller J, Lameyre J, Sabine PA, Schmid R, Sørensen H, Woolley AR (2002) Igneous rocks: a classification glossary of terms, Cambridge University Press, Cambridge, 236 p.

Lee CTA, Morton DM, Kistler RW, Baird AK (2007) Petrology and tectonics of Phanerozoic continent formation: from island arcs to accretion and continental arc magmatism, *Earth and Planetary Science Letters* 263:370–387.

Mahmoudi S, Corfu F, Masoudi F, Mehrabi B, Mohajjel M (2011) U–Pb dating and emplacement history of granitoid plutons in the Northern Sanandaj–Sirjan zone, Iran, *Journal of Asian Earth Sciences* 41:238–249.

Martin RF (2006) A-type granites of crustal origin ultimately result from open-system fenitization-type reactions in an extensional environment, *Lithos* 91:125–136.

Mason B, Moore CB (1982) Principles of geochemistry, John Wiley and Sons 344 p.

Masoudi F, Yardley BWD, Cliff RA (2002) Rb-Sr geochronology of pegmatites, plutonic rocks and a hornfels in the region southwest of Arak, *Iranian Journal of Sciences* 13:249–254.

Mazhari SA, Amini S, Ghalamghash J, Bea F (2009a) Petrogenesis of granitic unit of Naqadeh complex, Sanandaj–Sirjan Zone, NW Iran, *Arabian Journal of Geosciences* 4:59–67.

Mazhari SA, Bea F, Amini S, Ghalamghash J, Molina JF, Pillar M, Scarrow JH, Williams S (2009b) The Eocene bimodal Piranshahr massif of the Sanandaj- Sirjan zone, NW Iran. A marker of the end of the collision in the Zagros Orogen, *Journal of the Geological Society* 166:53–69.

McCall GJH, Kidd RGW (1982) The Makran, Southeastern Iran: The Anatomy of a Convergent Plate Margin Active from Cretaceous to Present, Geological Society, London, *Special Publications* 10:387–397.

Mehdipour Ghazi J, Moazzen M (2015) Geodynamic evolution of the Sanandaj-Sirjan Zone, Zagros Orogen, Iran, *Turkish Journal of Earth Sciences* 24:513-528.

Middlemost EAK (1994) Naming materials in the magma/igneous rock system, *Earth-science reviews* 37:215-224.

Miller CF, McDowell SM, Mapes RW (2003) Hot and cold granites? Implications of zircon saturation temperatures and preservation of inheritance, *Geology* 31:529–532.

Moayyed M (2013) Petrography and Petrology of A–type rhyolites of Ghaleh–chay (Ajabshir, East-Azerbaijan), *Iranian Journal of Crystallography and Mineralogy* 3:403–416 (in Persian).

Mohajjel M, Fergusson CL (2000) Dextral transpression in late-cretaceous continental collision, Sanandaj-Sirjan zone, Western Iran, *Journal of Structural Geology* 22:1125-1139.

Mohajjel M, Fergusson CL, Sahandi MR (2003) Cretaceous-Tertiary convergence and continental collision, Sanandaj-Sirjan zone, western Iran, *Journal of Asian Earth Sciences* 21:397–412.

Mohammadi A, Moazzen M, Lechmann A, Laurent O (2019) Zircon U-Pb geochronology and geochemistry of Late Devonian–Carboniferous granitoids in NW Iran: Implications for the opening of Paleo-Tethys, *International Geology Review* 62:1931–1948.

Pearce JA (1983) Role of the sub-continental lithosphere in magma genesis at active continental margins, in Hawkesworth CJ, Norry MJ, eds., Continental basalts

and mantle xenoliths: Nantwich, Cheshire, Shiva Publications, p. 230–249.

Pearce JA (1996) Sources and settings of granitic rocks, *Episodes* 19:120-125.

Pearce JA, Harris NBW, Tindle AG (1984) Trace-element discrimination diagrams for the tectonic interpretation of granitic-rocks, *Journal of Petrology* 25:956–983.

Rolland Y, Sosson M, Adamia S, Sadradze N (2011) Prolonged Variscan to Alpine history of an active Eurasian margin (Georgia, Armenia) revealed by 40Ar/39Ar dating, *Gondwana Research* 20:798–815.

Rollinson H (1993) Using Geochemical Data: Evaluation, Presentation, Interpretation, Harlow, England, Addison-Wesley/Longman 352 p.

Saccani E, Azimzadeh Z, Dilek Y, Jahangiri A (2013) Geochronology and petrology of the Early Carboniferous Misho Mafic Complex (NW Iran), and implications for the melt evolution of Paleo-Tethyan rifting in Western Cimmeria, *Lithos* 162:264–278.

Sengör AMC (1987) Tectonic of the Tethysides: Orogenic collage development in a collisional setting, *Annual Review of Earth and Planetary Sciences* 15:213-244.

Shafaii Moghadam H, Li XH, Ling XX, Stern RJ, Santos JF, Meinhold G, Ghorbani G, Shahabi H (2015) Petrogenesis and tectonic implications of Late Carboniferous A-type granites and gabbronorites in NW Iran: Geochronological and geochemical constraints, *Lithos* 212–215:266–279.

Shahabpour J (2007) Island-arc affinity of the Central Iranian Volcanic Belt, *Journal of Asian Earth Sciences* 30:652–665.

Shahabpour J (2010) Tectonic implications of the geochemical data from the Makran igneous rocks in Iran, *Island Arc* 19:676–689.

Shahbazi H, Siebel W, Pourmoafee M, Ghorbani M, Sepahi AA, Shang CK, Vosoughi Abedini M (2010) Geochemistry and U–Pb zircon geochronology of the Alvand plutonic complex in Sanandaj–Sirjan Zone (Iran): new evidence for Jurassic magmatism, *Journal of Asian Earth Sciences* 9:668–683.

Shakerardakani F, Neubauer F, Masoudi F, Mehrabi B, Liu X, Dong Y, Mohajjel M, Monfaredi B, Friedl G (2015) Panafrican basement and Mesozoic gabbro in the Zagros orogenic belt in the Dorud–Azna region (NW Iran): Laser-ablation ICP–MS zircon ages and geochemistry, *Tectonophysics* 647:146–171.

Sosson M, Rolland Y, Danelian T, Muller C, Melkonyan R, Adamia S, Kangarli T, Avagyan A, Galoyan G (2010) Subductions, obduction and collision in the Lesser Caucasus (Armenia Azerbaijan, Georgia), new insights. In: In: Sosson, M., Kaymakci, N., Stephenson, R.F., Bergerat, F., Starostenko, V. (Eds.), Sedimentary Basin Tectonics from the Black Sea and Caucasus to the Arabian Platform 340, Geological Society of London, pp. 329–352 Special Publication.

Stampfli G, Marcoux J, Baud A (1991) Tethyan margins in space and time, Palaeogeogr. Palaeoclimatol. *Palaeoecol*. 87:373-409.

Stampfli GM (2000) Tethyan oceans, Geological Society, London, S*pecial Publications* 173:1-23.

Stampfli GM, Borel GD (2002) A plate tectonic model for the Paleozoic and Mesozoic constrained by dynamic plate boundaries and restored synthetic oceanic isochrones, *Earth and Planetary Science Letters* 196:17–33.

Stocklin J (1968) Structural history and tectonics of Iran: A review, Am. Assoc. Pet. Geol. Bull. 52:1229-1258.

Sun SS, McDonough WF (1989) Chemical and isotopic systematics of oceanic basalts: Implications for mantle composition and processes, Geological Society, London, *Special Publications* 42:313–345.

Takin M (1972) Iranian geology and continental drift in the Middle East, *Nature* 235:147-150.

Tavakoli-Shirazi S, de Lamotte DF, Wrobel-Daveau JC, Ringenbach JC (2013) Pre-Permian uplift and diffuse extensional deformation in the High Zagros Belt (Iran): integration in the geodynamic evolution of the Arabian plate, *Arabian Journal of Geosciences* 6:2329-2342.

Taylor SR, McLennan SM (1995) The geochemical evolution of the continental crust, *Review of Geophysics* 33:241-265.

Thiele O, Alavi M, Assefi R, Hushmandzadeh A, Seyed-Emami K, Zahedi M (1968) Explanatory Text of the Golpaygan Quadrangle Map, Geological Survey of Iran.

Thirlwall MF, Smith TE, Graham AM, Theodorou N, Hollings P, Davidson JP, Arculus RD (1994) High field strength element anomalies in arc lavas: Source or processes, *Journal of Petrology* 35:819-838.

Topuz G, Altherr R, Siebel W, Schwarz WH, Zack T, Hasozbek A, Barth M, Satir M, Sen C (2010) Carboniferous high-potassium I-type granitoid magmatism in the Eastern Pontides: the Gumushane pluton (NE Turkey), *Lithos* 116:92–110.

Turner SP, Foden JD, Morrison RS (1992) Derivation of some A-type magmas by fractionation of basaltic magma- an example from the Padthaway Ridge, South Australia, *Lithos* 28:151–179.

Verdel C, Wernicke BP, Hassanzadeh J, Guest B (2011) A Paleogene extensional arc flare-up in Iran, Tectonics 30:TC3008.

von Raumer JF, Stampfli GM, Bussy F (2003) Gondwana-derived microcontinents-The constituents of the Variscan and Alpine collisional orogens, *Tectonophysics* 365:7–22.

Watson EB, Harrison TM (1983) Zircon saturation revisited, *EPSL* 64:295–304.

Weaver BL (1991) The origin of ocean-island basalts endmember composition: trace element and isotopic constraints, *Earth and Planetary Science Letters* 104:381–397.

Whalen JB, Currie KL, Chappell BW (1987) A-type granites - geochemical characteristics, discrimination

and petrogenesis, *Contributions to Mineralogy and Petrology* 95:407–419.

Whalen JB, Jenner GA, Longstaff FJ, Robert F, Galiepy C (1996) Geochemical and isotopic (O, Nd, Pb and Sr) constraints on A-type granite petrogenesis based on the Topsails igneous suite, Newfoundland Appalachians, *Journal of Petrology* 31:1463–1489.

Yang JH, Wu FY, Chung SL, Wilde SA, Chu MF (2006) A hybrid origin for the Qianshan A-type granite, northeast China: geochemical and Sr–Nd–Hf isotopic evidence, *Lithos* 89:89–106.